Collective excitations of hard-core Bosons at half filling on square and triangular lattices: Development of roton minima and collapse of roton gap

Tyler Bryant and Rajiv R. P. Singh
Department of Physics, University of California, Davis, CA 95616, USA
(Dated: February 1, 2008)

We study ground state properties and excitation spectra for hard-core Bosons on square and triangular lattices, at half filling, using series expansion methods. Nearest-neighbor repulsion between the Bosons leads to the development of short-range density order at the antiferromagnetic wavevector, and simultaneously a roton minima in the density excitation spectra. On the square-lattice, the model maps on to the well studied XXZ model, and the roton gap collapses to zero precisely at the Heisenberg symmetry point, leading to the well known spectra for the Heisenberg antiferromagnet. On the triangular-lattice, the collapse of the roton gap signals the onset of the supersolid phase. Our results suggest that the transition from the superfluid to the supersolid phase maybe weakly first order. We also find several features in the density of states, including two-peaks and a sharp discontinuity, which maybe observable in experimental realization of such systems.

PACS numbers:

I. INTRODUCTION

A microscopic theory for rotons in the excitation spectra of superfluids was first developed by Feynman, where he showed that the roton minima was related to a peak in the static structure factor.[1] This study has had broad impact in condensed matter physics ranging from Quantum Hall Effect[2] to frustrated antiferromagnets.[3,4,5] In recent years considerable interest has also centered on Supersolid phases of matter.[6] While the existence of such homogeneous bulk phases in Helium remains controversial,[7,8] in case of lattice models such phases have been clearly established. One such example is that of hard-core Bosons hopping on a triangular-lattice, where a large enough nearest-neighbor repulsion leads to supersolid order.[9,10,11,12,13,14] The nature of the excitation spectra in the superfluid phase and on approach to the supersolid transition has not been addressed for the spin-half model.

Here we use series expansion methods to study the ground state properties and excitation spectra of hard-core Bosons, at half filling, on square and triangular lattices, with nearest neighbor repulsion. On the square-lattice, the model is equivalent to the antiferromagnetic XXZ model, and we present the elementary excitation spectra for the XXZ model with XY type anisotropy. To our knowledge this calculation has not been done before. It should be useful for experimental studies of antiferromagnetic materials with XY anisotropy. We set the XY coupling to unity and study the spectra as a function of the Ising coupling J_z. For the XY model, the spectra is gapless at $q = 0$ (the Goldstone mode of the superfluid) and has a maximum at the antiferromagnetic wavevector (π, π). As the Ising coupling is increased a roton minima develops at the antiferromagnetic wavevector, which goes to zero at the point of Heisenberg symmetry ($J_z = 1$), as expected for the system with doubled unit cell.

For the triangular-lattice, the hard-core Boson model maps onto a ferromagnetic XY model, which is unfrustrated. The nearest-neighbor repulsion, on the other hand corresponds to an antiferromagnetic Ising coupling, which is frustrated. This model cannot be mapped onto an *antiferromagnetic* XXZ model on the triangular lattice. For this model, we calculate the equal-time structure factor $S(q)$ as well as the excitation spectra, $\omega(q)$. Once again, we find that in the absence of nearest-neighbor repulsion, the excitation spectra is gapless at $q = 0$ and has a maximum at the antiferromagnetic wavevector ($(4\pi/3, 0)$ and equivalent points). As the repulsion is increased, a pronounced peak develops in $S(q)$ at these wavevectors and simultaneously a sharp roton minima develops in the spectra. Series extrapolations suggest that the roton gap vanishes when the repulsion term (J_z) reaches a value of ≈ 4.5. However, we are unable to estimate any critical exponents for the vanishing of the gap or for the divergence of the structure factor. A comparison of our structure factor data with the Quantum Monte Carlo data of Wessel and Troyer, leads us to suggest that the transition to the supersolid phase maybe weakly first order and occurs for a value of J_z slightly less than 4.5.

Our calculations also show a near minimum and flat regions in the spectra at the wavevectors $(\pi, \pi/\sqrt{3})$, which correspond to the midpoint of the faces of the Brillouin zone. These are points where the antiferromagnetic Heisenberg model has a well defined minima.[4] In our case the dispersion is very flat along some directions and a minimum along others. There are several distinguishing features in the density of states (DOS) of the excitation spectra. The largest maximum in the DOS is close to the maximum excitation energy and is not unlike many other antiferromagnets. But, here, in addition, we get a second maximum in the DOS from the flat regions in the spectra at the midpoint of the faces of the Brillouin zone and a sharp drop in the DOS at the roton energy. It maybe possible to engineer such hard-core Boson systems on a triangular-lattice in cold atomic gases. It should, then, be possible to excite these collective exciations either op-

tically or by driving the system out of equilibrium. A measurement of the energies associated with the characteristic features in the density of states can be used to accurately determine the microscopic parameters of the system.

II. METHOD

The linked-cluster series expansions performed here involve writing the Hamiltonian of interest as

$$\mathcal{H} = \mathcal{H}_0 + \lambda \mathcal{H}_1 \tag{1}$$

where the eigenstates of $\mathcal{H}_0$ define the basis to be used and $\mathcal{H}_1$ is the perturbation to be applied in a linked cluster expansion. Ground state properties are then obtained as a power series in λ using Raleigh-Schrodinger perturbation theory.

Excited state properties are obtained following the procedure outlined in[22], in which a similarity transformation is obtained in order to block diagonalize the Hamiltonian where the ground state sits in a block by itself and the one-particle states form another block.

$$\mathcal{H}^{\rm eff} = \mathcal{S}^{-1}\mathcal{H}\mathcal{S} \tag{2}$$

where $\mathcal{H}^{\rm eff}$ is an effective Hamiltonian for the states which are the perturbatively constructed extensions of the single spin-flip states. The effective Hamiltonian is then used to obtain a set of transition amplitudes $\sum_{r=0}\lambda^r c_{r,m,n}$ that describe propagation of the excitation through a distance $(m\hat{x}+n\hat{y})$ for the square lattice and $(\frac{1}{2}m\hat{x}+\frac{\sqrt{3}}{2}n\hat{y})$ with m and n both even or both odd for the triangular lattice.

These transition amplitudes are used to obtain the transition amplitudes for the bulk lattice by summing over clusters. Fourier transformation of the bulk transition amplitudes then gives the excitation energy in momentum space.

$$\Delta(q_x,q_y) = \sum_{r=0}\lambda^r \sum_{m,n} c_{r,m,n} f_{m,n}(q_x,q_y) \tag{3}$$

where $f_{m,n}(q_x,q_y)$ is given by the symmetry of the lattice, with

$$\begin{aligned} f^{\rm sqr}_{m,n}(q_x,q_y) = [&cos(mq_x+nq_y)+cos(mq_x-nq_y) \\ &+cos(nq_x+mq_y)+cos(nq_x-mq_y)]/4 \end{aligned} \tag{4}$$

for the square lattice and

$$\begin{aligned} f^{\rm tri}_{m,n}(q_x,q_y) = \Bigg[&cos(\frac{m}{2}q_x)cos(\frac{n\sqrt{3}}{2}q_y) \\ &+ cos(\frac{\sqrt{3}(m+n)}{4}q_y)cos(\frac{m-3n}{4}q_x) \\ &+ cos(\frac{\sqrt{3}(m-n)}{4}q_y)cos(\frac{m+3n}{4}q_x)\Bigg]/3 \end{aligned} \tag{5}$$

for the triangular lattice.

In order to access values of the expansion parameter λ up to and including $\lambda = 1$, we use standard first order integrated differential approximants[18] (IDAs) of the form

$$Q_L(x)\frac{df}{dx} + R_M(x)f + S_T(x) = 0 \tag{6}$$

where Q_L,R_M,S_T are polynomials of degree L,M,and T determined uniquely from the expansion coefficients.

When gapless modes are present, estimates of the spin-wave velocity are made using the technique of Singh and Gelfand[15]. For small $q = |\mathbf{q}|$ the spectrum is assumed to have the form $\Delta(\mathbf{q}) \sim [A(\lambda)+B(\lambda)q^2]^{1/2}$. To calculate the spin-wave velocity, we expand $\Delta(\mathbf{q})$ in powers of q, $\Delta(q) = C(\lambda)+D(\lambda)q^2+...$ and identify $C = A^{1/2}$ and $D = B/2A^{1/2}$. Thus the series $2C(\lambda)D(\lambda)$ provides an estimate for B, which is the square of the spin-wave velocity.

III. SQUARE LATTICE

On the square lattice we perform two distinct types of expansions. For $J_z \geq J_\perp$, one can expand directly in $J_\perp/J_z$ by choosing

$$\begin{aligned} \mathcal{H}_0 &= \sum_{<i,j>} S^z_i S^z_j \\ \mathcal{H}_1 &= \sum_{<i,j>} (S^x_i S^x_j + S^y_i S^y_j) \end{aligned} \tag{7}$$

In this case λ in (1) is $J_\perp$ (setting $J_z = 1$). Since $\mathcal{H}_1$ conserves the total S^z, one can perform the computation to high order by restricting the full Hilbert space to the total S^z sector of interest, which in this paper will be restricted to total $S^z = 0$ (half filling).

Series expansion studies of the excitation spectra by Singh et al.[15] and subsequently extended by Zheng et al.[16] have been performed for $J_z \geq J_\perp$, with expansions involving linked clusters of up to 11 sites (λ^{10}) and 15 sites (λ^{14}) respectively.

Fig. 1 shows the results of the spin-wave dispersion analysis for $J_\perp$ from the dispersionless Ising model $J_\perp = 0$ to the Heisenberg model $J_\perp = 1$. One can see the development of minima at $(0,0)$ and (π,π) with increasing $J_\perp$, with the gap completely closing at $J_\perp = 1$. Since IDAs are not accurate near the gapless points, the dotted line shows the estimated spin-wave velocity $v = 1.666$ when $J_\perp = 1$.

To obtain the spectra with XY anisotropy ($J_z \leq J_\perp$), we need to develop a different type of expansion. We consider the following break up of the Hamiltonian: (for $J_z \leq J_\perp$)

$$\begin{aligned} \mathcal{H}_0 &= \sum_{<i,j>} S^x_i S^x_j \\ \mathcal{H}_1 &= \sum_{<i,j>} (S^y_i S^y_j + J_z S^z_i S^z_j) \end{aligned} \tag{8}$$

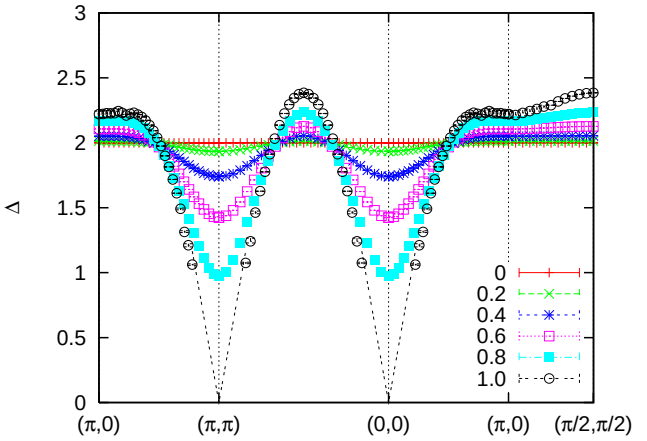

FIG. 1: (Color online) The spin-wave dispersion of the XXZ model on the square lattice for various values of $J_\perp$ ($J_z = 1$). The error bars give an indication of the spread of various IDAs. The lines around the gapless points for $J_\perp = 1$ show the calculated spin-wave velocity.

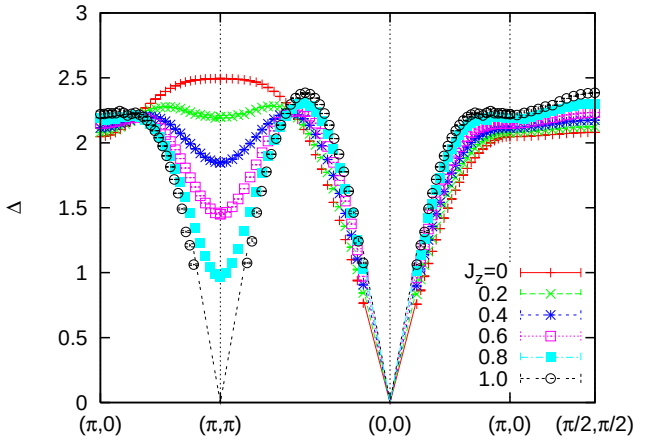

FIG. 2: (Color online) The spin-wave dispersion of the XXZ model on the square lattice for various values of J_z ($J_\perp = 1$). The error bars give an indication of the spread of various IDAs. The lines around the gapless points show the calculated spin-wave velocities.

where $J_\perp = 1$. Now, a new series is obtained for each value of J_z, and the XXZ model is only obtained upon extrapolation to $\lambda = 1$. In contrast to the first type of expansion, $\mathcal{H}_1$ does not conserve total S^z, and so the entire Hilbert space must be used, limiting the order of computation of the series to λ^{10} (11 sites).

Fig. 2 shows the results of the spin-wave dispersion analysis for several values of J_z from the XY model ($J_z = 0$) to the Heisenberg model ($J_\perp = 1$). We find that for the pure XY model, there is gapless excitations at $q = 0$ (Goldstone modes of the superfluid phase), but there is no roton minima at the antiferromegnetic wavevector. As J_z is increased, the spin-wave velocity increases and a clear roton-minima develops at the antiferromagnetic wavevector. This minima collapses to zero as the Heisenberg point is approached. In fact, the doubling of the unit cell implies that for the Heisenberg limit, the spectra at q and at $q+(\pi,\pi)$ become identical. Another point of interest is that along the direction $(\pi, 0)$ to $(\pi/2, \pi/2)$, which corresponds to the antiferromagnetic zone boundary, the dispersion is very flat for the pure XY model. A weak minimum develops at $(\pi, 0)$ as the Heisenberg symmetry point is reached. These results should be useful in comparing with spectra of two-dimensional antiferromagnets, where there is significant exchange anisotropy.

IV. TRIANGULAR LATTICE

There has been much recent interest in the XXZ model on the triangular lattice. The spin-$\frac{1}{2}$ XXZ model with ferromagnetic in-plane coupling $J_\perp < 0$ and antiferromagnetic coupling in the z direction $J_z > 0$ can be mapped to a hard-core boson model with nearest neighbor repulsion.

TABLE I: Series coefficients for the ground state energy per site E_0/N and M

n	E_0/N for J_z=0	M for J_z=0
0	-5.000000e-01	1.250000e-01
2	-4.166667e-02	-6.944444e-03
4	-4.282407e-03	-2.267072e-03
6	-1.251190e-03	-1.141688e-03
8	-5.538567e-04	-7.184375e-04
10	-2.990401e-04	-5.039687e-04
12	-1.823004e-04	-3.784068e-04
14	-1.015895e-04	-2.494459e-04

$$\mathcal{H}_b = -t \sum_{<i,j>} (b_i^\dagger b_j + b_i b_j^\dagger) + V \sum_{<i,j>} n_i n_j \qquad (9)$$

where $b_i^\dagger$ is the bosonic creation operator, $n_i = b_i^\dagger b_i$. The parameters are related by $t = -J_\perp/2$ and $V = J_z$. For the rest of this section, we let $J_\perp = -1$, and so $V/t = -2J_z/J_\perp = 2J_z$.

We will continue to use the spin language as it is natural for our study. For $J_z = 0$, the ferromagnetic in-plane coupling is unfrustrated. As J_z is increased, the competing interaction leads to an emergence of a supersolid order.

We have performed expansions for the triangular lattice XXZ model of the form

$$\begin{aligned} \mathcal{H}_0 &= -\sum_{<i,j>} S_i^x S_j^x \\ \mathcal{H}_1 &= \sum_{<i,j>} (-S_i^y S_j^y + J_z S_i^z S_j^z) \end{aligned} \qquad (10)$$

where $J_\perp = -1$. Series are obtained for each value of

J_z, and the XXZ model is obtained upon extrapolation to $\lambda = 1$.

The static structure factor

$$S(\mathbf{k}) = \sum_{\mathbf{r}} e^{i\mathbf{k}\cdot\mathbf{r}} \langle S_0^z S_{\mathbf{r}}^z \rangle \qquad (11)$$

is shown in Fig. 3 along contours shown in Fig. 4. As J_z increases, a peak forms at wavevector $\mathbf{q}$=$(4\pi/3, 0)$. A plot of this point is shown in fig. 5 along with QMC data from Wessel and Troyer.[10]

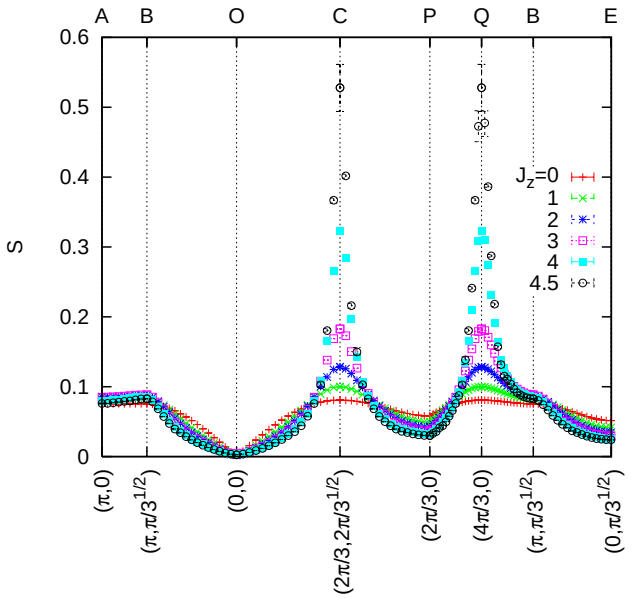

FIG. 3: (Color online) The static structure factor of the XXZ model on the triangular lattice for various values of J_z ($J_\perp$=-1). The error bars give an indication of the spread of IDAs.

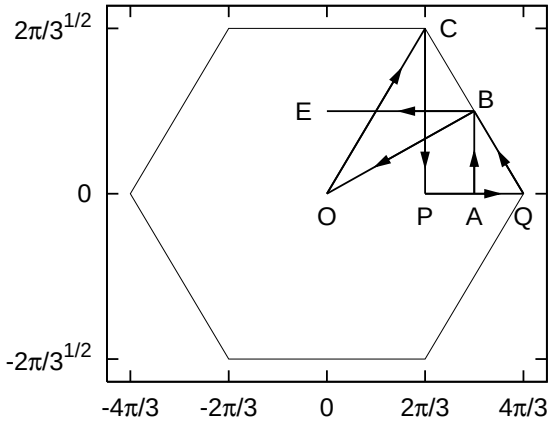

FIG. 4: The hexagonal first Brillouin zone of the triangular lattice and the path ABOCPQBE along which the static structure factor and spin-wave dispersion have been plotted in Figs. 3 and 6.

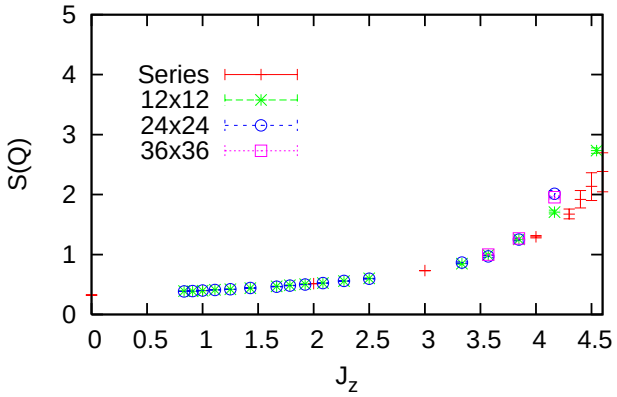

FIG. 5: (Color online) The static structure factor at $\mathbf{q}$=$(4\pi/3, 0)$ of the XXZ model on the triangular lattice versus J_z ($J_\perp$=-1). The error bars for the series data give an indication of the spread of IDAs. Also shown are QMC data for 12x12,24x24,and 36x36 site clusters from Wessel and Troyer.[10]

Fig. 6 shows the results of the spin-wave dispersion analysis for various values of J_z ($J_\perp = -1$). The error bars give an indication of the spread of IDAs. The lines around the gapless points show the calculated spin-wave velocities. One can see the development of minima at $\mathbf{Q}$ with increasing J_z, with the gap completely closing at $J_z \sim 4.5$. Since IDAs are not accurate near the gapless point ($q = 0$), the dotted line shows the estimated spin-wave velocities.

We have been unable to get any consistent estimates for the critical exponents characterizing the divergence of the antiferromagnetic structure factor and the vanishing of the roton gap as the supersolid phase is approached. Furthermore, the comparison with the QMC data of Wessel and Troyer show that the QMC data begin to show deviations from our series expansion results before $J_z = 4.5$. We believe, this implies that the superfluid to supersolid transition is weakly first order. Wessel and Troyer estimate the transition to be at $J_z \approx 4.3 \pm 0.2$ ($|t/V| = 0.115 \pm 0.005$). Note that the spin-wave theory gives the transition point to be at $J_z = 2$,[9] so that quantum fluctuations play a substantial role here. Additional QMC studies, should provide further insight into the nature of the transition.[24]

The calculations also show that near the midpoint of the faces of the Brillouin Zone (point B in Fig. 4), the dispersion is a minima in the direction perpendicular to the zone face QB and is very flat in other directions. This behavior is reminiscent of the dispersion in the Heisenberg antiferromagnet on the traingular lattice where there is a true minimum at this point.[4,5] Note that this behavior is unrelated to any peak in the static structure factor and thus, as in case of the Heisenberg model, is more quantum mechanical in nature.

In Fig. 7, we show the density of states for the spectra

for $J_z = 2$. There are several distinguishing features in the density of states. First the largest peak in the density of states occurs close to the highest excitation energies. This is not unlike what is found in many other antiferromegnets. However, here, there is a second peak that corresponds to the flat regions in the spectra near the point B. Finally, at the roton energy there is a sharp drop in the density of states. The only contributions to the density of states below the roton gap comes from the Goldstone modes near $q = 0$. Since the latter have very small density of states, there is a discontinuity in the density of states at the roton energy.

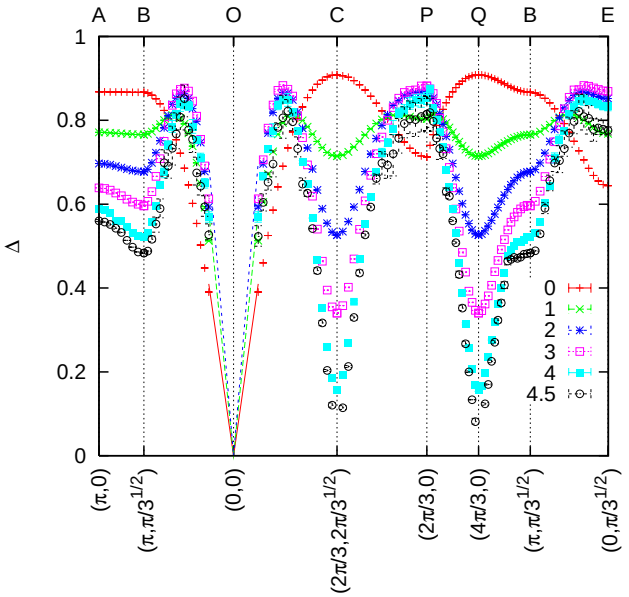

FIG. 6: (Color online) The spin-wave dispersion of the XXZ model on the triangular lattice for various values of J_z ($J_\perp = -1$). The error bars give an indication of the spread of IDAs. The lines around the gapless points show the calculated spin-wave velocities.

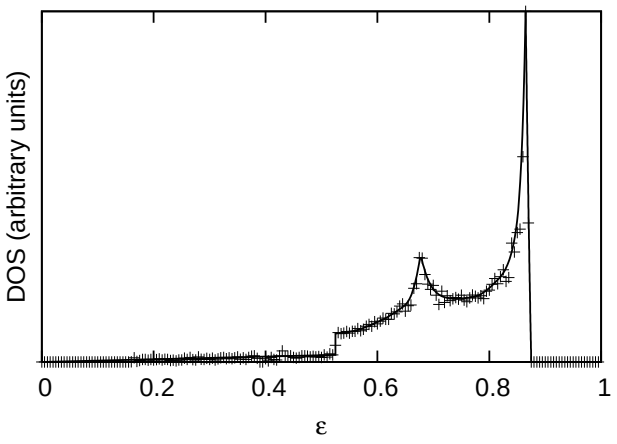

FIG. 7: The density of states for the XXZ model on the triangular lattice for $J_z = 2$ ($J_\perp = -1$).

V. SUMMARY AND CONCLUSIONS

In this paper, we have studied the excitation spectra of hard-core Boson models at half-filling on square and triangular lattices. The calculations show the development of the roton minima at the antiferromagnetic wavevector, due to nearest-neighbor repulsion. In accord with Feynman's ideas, the development of the minima is correlated with the emergence of a sharp peak in the static structure factor. The case of triangular-lattice is clearly more interesting as one has a phase transition from a superfluid to a supersolid phase, where the roton gap goes to zero. Our series results suggest that the roton-gap vanishes at $J_z \approx 4.5$. However, there maybe a weakly first order transition slightly before this J_z value. A more careful finite-size scaling analysis of the QMC data should provide further insight into this issue.

Our results of the spectra suggest two peaks in the density of states and a sharp drop in the density of states at the energy of the roton minima. If such a hard-core Boson system on a triangular-lattice is realized in cold-atom experiments, a measurement of the two peaks in the density of states and the roton minima can be used to determine independently the hopping parameter t and the nearest-neighbor repulsion V.

Acknowledgments

This research is supported in part by the National Science Foundation Grant Number DMR-0240918. We are greatful to Stefan Wessel for providing us with the QMC data for the structure factors and to Marcos Rigol and Stefan Wessel for discussions.

[1] R. P. Feynman, Phys. Rev. **94**, 262 (1954).
[2] S. M. Girvin, A. H. MacDonald, and P. M. Platzman Phys. Rev. Lett. **54**, 581-583 (1985).
[3] P.Chandra, P. Coleman and A.I. Larkin, J. Phys. Cond. Matter 2, 7933 (1990).
[4] W. Zheng, *et al*, Phys. Rev. Lett. **96**, 057201 (2006); Phys. Rev. B 74, 224420 (2006).
[5] O. A. Starykh, A. V. Chubukov and A. G. Abanov, Phys Rev. B**74**, 180403 (2006); A. L. Chernyshev and M. E. Zhitomirsky, Phys. Rev. Lett. **97**, 207202 (2006).
[6] E. Kim and M. H. W. Chan, Nature 427, 225 (2004).
[7] See for example M. Boninsegni *et al*, Phys. Rev. Lett. **97**, 080401 (2006).
[8] P. W. Anderson, W. F. Brinkman, D. A. Huse, Science **310**, 1164 (2005).
[9] G. Murthy, D. Arovas, and A. Auerbach, Phys. Rev. B, **55**, 3104 (1997).
[10] S. Wessel and M. Troyer, Phys. Rev. Lett. **95**, 127205 (2005).
[11] D. Heidarian and K. Damle, Phys. Rev. Lett. **95**, 127206 (2005).
[12] R. G. Melko, A. Paramekanti, A. A. Burkov, A. Vishwanath, D.N. Sheng, and L. Balents Phys. Rev. Lett. **95**, 127207 (2005).
[13] M. Boninsegni and N. Prokof'ev Phys. Rev. Lett. **95**, 237204 (2005).
[14] E. Zhao and Arun Paramekanti Phys. Rev. Lett. **96**, 105303 (2006).
[15] Rajiv R. P. Singh, Martin P. Gelfand, Phys. Rev. B, **52**, R15 695 (1995)
[16] W. Zheng, J. Oitmaa, and C.J. Hamer, Phys. Rev. B, **71**, 184440 (2005).
[17] W. Zheng, J. Oitmaa, and C.J. Hamer, Phys. Rev. B, **43**, 8321 (1991).
[18] J. Oitmaa, C. Hamer, and W. Zheng, *Series Expansion Methods for Strongly Interacting Lattice Models* (Cambridge: Cambridge University Press) (2006).
[19] A. W. Sandvik and R. R. P. Singh, Phys. Rev. Lett., **86**, 528 (2001).
[20] W. Zheng, C.J. Hamer, R. R. P. Singh, S. Trebst and H. Monien, Phys. Rev. B, **63**, 144410 (2001).
[21] H.-Q. Lin, J. S. Flynn and D. D. Betts, Phys. Rev. B, **64**, 214411 (2001).
[22] M. P. Gelfand and R. R. P. Singh, Adv. Phys. **49**, 93 (2000).
[23] T. Bryant, Ph.D. Dissertation, University of California, Davis, to be submitted.
[24] S. Wessel, to be published.

TABLE II: Series coefficients for the magnon dispersion on the square lattice for $J_z = 0$ (XY model), nonzero coefficients up to r=9 are listed for compactness (the complete series can be found in Ref. 23)

(r,m,n)	$c_{r,m,n}$	(r,m,n)	$c_{r,m,n}$	(r,m,n)	$c_{r,m,n}$	(r,m,n)	$c_{r,m,n}$
(0,0,0)	2.000000e+00	(3,2,1)	-7.291667e-02	(8,3,3)	-1.715283e-03	(9,5,2)	-1.334928e-03
(2,0,0)	-4.166667e-02	(5,2,1)	-1.968093e-02	(4,4,0)	-2.712674e-03	(8,5,3)	-7.225832e-04
(4,0,0)	-1.023582e-02	(7,2,1)	-8.897152e-03	(6,4,0)	-2.980614e-03	(9,5,4)	-3.993759e-04
(6,0,0)	-5.390283e-03	(9,2,1)	-4.845897e-03	(8,4,0)	-1.932294e-03	(6,6,0)	-1.156309e-04
(8,0,0)	-2.781363e-03	(4,2,2)	-1.627604e-02	(5,4,1)	-5.303277e-03	(8,6,0)	-3.216877e-04
(1,1,0)	-1.000000e+00	(6,2,2)	-5.758412e-03	(7,4,1)	-4.614353e-03	(7,6,1)	-3.803429e-04
(3,1,0)	4.340278e-02	(8,2,2)	-2.558526e-03	(9,4,1)	-3.055177e-03	(9,6,1)	-6.801940e-04
(5,1,0)	1.811921e-02	(3,3,0)	-1.215278e-02	(6,4,2)	-3.468926e-03	(8,6,2)	-3.612916e-04
(7,1,0)	7.679634e-03	(5,3,0)	-7.265535e-03	(8,4,2)	-2.946432e-03	(9,6,3)	-2.662506e-04
(9,1,0)	4.056254e-03	(7,3,0)	-3.368594e-03	(7,4,3)	-1.901715e-03	(7,7,0)	-2.716735e-05
(2,1,1)	-2.500000e-01	(9,3,0)	-1.895272e-03	(9,4,3)	-1.807997e-03	(9,7,0)	-1.043517e-04
(4,1,1)	-2.314815e-02	(4,3,1)	-2.170139e-02	(8,4,4)	-4.516145e-04	(8,7,1)	-1.032262e-04
(6,1,1)	-5.841368e-03	(6,3,1)	-1.033207e-02	(5,5,0)	-5.303277e-04	(9,7,2)	-1.141074e-04
(8,1,1)	-1.566143e-03	(8,3,1)	-4.852573e-03	(7,5,0)	-1.004891e-03	(8,8,0)	-6.451636e-06
(2,2,0)	-1.250000e-01	(5,3,2)	-1.060655e-02	(9,5,0)	-9.122910e-04	(9,8,1)	-2.852685e-05
(4,2,0)	-3.067130e-02	(7,3,2)	-6.456544e-03	(6,5,1)	-1.387570e-03	(9,9,0)	-1.584825e-06
(6,2,0)	-9.598676e-03	(9,3,2)	-3.716341e-03	(8,5,1)	-1.771298e-03		
(8,2,0)	-3.989385e-03	(6,3,3)	-2.312617e-03	(7,5,2)	-1.141029e-03		

TABLE III: Series coefficients for the ground state energy per site E_0/N and M

n	E_0/N for J_z=0	M for J_z=0	E_0/N for J_z=1	M for J_z=1	E_0/N for J_z=2	M for J_z=2
0	-7.500000e-01	-2.500000e-01	-7.500000e-01	-2.500000e-01	-7.500000e-01	-2.500000e-01
1	0.000000e+00	0.000000e+00			0.000000e+00	0.000000e+00
2	-3.750000e-02	7.500000e-03	-1.500000e-01	3.000000e-02	-3.375000e-01	6.750000e-02
3	-7.500000e-03	3.000000e-03			6.750000e-02	-2.700000e-02
4	-3.102679e-03	1.989902e-03	-6.428572e-04	3.271769e-03	-3.081696e-02	3.263208e-02
5	-1.557668e-03	1.356060e-03			4.457109e-02	-4.706087e-02
6	-9.211778e-04	1.018008e-03	-1.686432e-03	2.253907e-03	-5.708928e-02	7.245005e-02
7	-5.949646e-04	7.975125e-04			7.181401e-02	-1.117528e-01
8	-4.102048e-04	6.468307e-04	-7.027097e-04	1.498661e-03	-1.001587e-01	1.839365e-01
9	-2.965850e-04	5.380214e-04			1.440002e-01	-3.025679e-01
10	-2.225228e-04	4.565960e-04	-3.752974e-04	1.029273e-03	-2.164303e-01	5.141882e-01
11	-1.719314e-04	3.937734e-04			3.343757e-01	-8.849178e-01
12	-1.360614e-04	3.441169e-04	-2.322484e-04	7.779323e-04	-5.294397e-01	1.545967e+00

TABLE IV: Series coefficients for the magnon dispersion on the triangular lattice $J_z = 0$, $J_\perp = -1$, nonzero coefficients up to r=9 are listed for compactness (the complete series can be found in Ref. 23)

(r,m,n)	$c_{r,m,n}$	(r,m,n)	$c_{r,m,n}$	(r,m,n)	$c_{r,m,n}$	(r,m,n)	$c_{r,m,n}$
(0,0,0)	3.000000e+00	(6,5,1)	-6.186994e-03	(5,8,0)	-2.318836e-03	(9,10,6)	-3.135408e-05
(2,0,0)	-3.125000e-02	(7,5,1)	-4.204807e-03	(6,8,0)	-2.496675e-03	(9,10,8)	-4.493212e-07
(3,0,0)	6.927083e-03	(8,5,1)	-3.031857e-03	(7,8,0)	-2.214348e-03	(6,11,1)	-9.073618e-05
(4,0,0)	-5.786823e-03	(9,5,1)	-2.274746e-03	(8,8,0)	-1.849982e-03	(7,11,1)	-2.637766e-04
(5,0,0)	-2.071746e-03	(4,5,3)	-3.466797e-03	(9,8,0)	-1.528161e-03	(8,11,1)	-3.828143e-04
(6,0,0)	-2.263644e-03	(5,5,3)	-4.350420e-03	(5,8,2)	-1.098718e-03	(9,11,1)	-4.387479e-04
(7,0,0)	-1.418733e-03	(6,5,3)	-3.723124e-03	(6,8,2)	-1.554950e-03	(7,11,3)	-7.642054e-05
(8,0,0)	-1.158308e-03	(7,5,3)	-2.959033e-03	(7,8,2)	-1.579331e-03	(8,11,3)	-1.651312e-04
(9,0,0)	-8.857566e-04	(8,5,3)	-2.305863e-03	(8,8,2)	-1.427534e-03	(9,11,3)	-2.316277e-04
(1,2,0)	-1.500000e+00	(9,5,3)	-1.817374e-03	(9,8,2)	-1.241335e-03	(8,11,5)	-1.824976e-05
(2,2,0)	-2.500000e-01	(3,6,0)	-7.265625e-03	(6,8,4)	-2.268405e-04	(9,11,5)	-4.925111e-05
(3,2,0)	2.236979e-02	(4,6,0)	-1.113487e-02	(7,8,4)	-4.458355e-04	(9,11,7)	-1.797285e-06
(4,2,0)	-3.470238e-03	(5,6,0)	-7.839022e-03	(8,8,4)	-5.558869e-04	(6,12,0)	-1.512270e-05
(5,2,0)	6.223272e-03	(6,6,0)	-5.440344e-03	(9,8,4)	-5.861054e-04	(7,12,0)	-9.486853e-05
(6,2,0)	2.258837e-03	(7,6,0)	-3.834575e-03	(7,8,6)	-1.528411e-05	(8,12,0)	-1.917140e-04
(7,2,0)	2.729869e-03	(8,6,0)	-2.794337e-03	(8,8,6)	-6.113630e-05	(9,12,0)	-2.589374e-04
(8,2,0)	1.793769e-03	(9,6,0)	-2.110041e-03	(9,8,6)	-1.121505e-04	(7,12,2)	-4.585233e-05
(9,2,0)	1.431100e-03	(4,6,2)	-5.200195e-03	(5,9,1)	-5.493588e-04	(8,12,2)	-1.209317e-04
(2,3,1)	-1.875000e-01	(5,6,2)	-5.161886e-03	(6,9,1)	-1.094328e-03	(9,12,2)	-1.836224e-04
(3,3,1)	-5.677083e-02	(6,6,2)	-4.187961e-03	(7,9,1)	-1.233659e-03	(8,12,4)	-2.281220e-05
(4,3,1)	-2.743217e-02	(7,6,2)	-3.218811e-03	(8,9,1)	-1.182811e-03	(9,12,4)	-5.685542e-05
(5,3,1)	-1.275959e-02	(8,6,2)	-2.454043e-03	(9,9,1)	-1.066119e-03	(9,12,6)	-4.193665e-06
(6,3,1)	-8.214468e-03	(9,6,2)	-1.905072e-03	(6,9,3)	-3.024539e-04	(7,13,1)	-1.528411e-05
(7,3,1)	-4.959005e-03	(5,6,4)	-5.493588e-04	(7,9,3)	-5.232866e-04	(8,13,1)	-6.113630e-05
(8,3,1)	-3.456161e-03	(6,6,4)	-1.094328e-03	(8,9,3)	-6.255503e-04	(9,13,1)	-1.121505e-04
(9,3,1)	-2.443109e-03	(7,6,4)	-1.233659e-03	(9,9,3)	-6.426095e-04	(8,13,3)	-1.824976e-05
(2,4,0)	-9.375000e-02	(8,6,4)	-1.182811e-03	(7,9,5)	-4.585233e-05	(9,13,3)	-4.925111e-05
(3,4,0)	-4.916667e-02	(9,6,4)	-1.066119e-03	(8,9,5)	-1.209317e-04	(9,13,5)	-6.290497e-06
(4,4,0)	-2.605934e-02	(4,7,1)	-3.466797e-03	(9,9,5)	-1.836224e-04	(7,14,0)	-2.183444e-06
(5,4,0)	-1.289340e-02	(5,7,1)	-4.350420e-03	(8,9,7)	-2.607109e-06	(8,14,0)	-1.878307e-05
(6,4,0)	-8.269582e-03	(6,7,1)	-3.723124e-03	(9,9,7)	-1.376709e-05	(9,14,0)	-4.937808e-05
(7,4,0)	-5.280757e-03	(7,7,1)	-2.959033e-03	(5,10,0)	-1.098718e-04	(8,14,2)	-9.124881e-06
(8,4,0)	-3.753955e-03	(8,7,1)	-2.305863e-03	(6,10,0)	-4.726374e-04	(9,14,2)	-3.135408e-05
(9,4,0)	-2.735539e-03	(9,7,1)	-1.817374e-03	(7,10,0)	-7.110879e-04	(9,14,4)	-6.290497e-06
(3,4,2)	-2.179687e-02	(5,7,3)	-1.098718e-03	(8,10,0)	-7.825389e-04	(8,15,1)	-2.607109e-06
(4,4,2)	-1.596136e-02	(6,7,3)	-1.554950e-03	(9,10,0)	-7.669912e-04	(9,15,1)	-1.376709e-05
(5,4,2)	-9.470639e-03	(7,7,3)	-1.579331e-03	(6,10,2)	-2.268405e-04	(9,15,3)	-4.193665e-06
(6,4,2)	-6.186994e-03	(8,7,3)	-1.427534e-03	(7,10,2)	-4.458355e-04	(8,16,0)	-3.258886e-07
(7,4,2)	-4.204807e-03	(9,7,3)	-1.241335e-03	(8,10,2)	-5.558869e-04	(9,16,0)	-3.685726e-06
(8,4,2)	-3.031857e-03	(6,7,5)	-9.073618e-05	(9,10,2)	-5.861054e-04	(9,16,2)	-1.797285e-06
(9,4,2)	-2.274746e-03	(7,7,5)	-2.637766e-04	(7,10,4)	-7.642054e-05	(9,17,1)	-4.493212e-07
(3,5,1)	-2.179687e-02	(8,7,5)	-3.828143e-04	(8,10,4)	-1.651312e-04	(9,18,0)	-4.992458e-08
(4,5,1)	-1.596136e-02	(9,7,5)	-4.387479e-04	(9,10,4)	-2.316277e-04		
(5,5,1)	-9.470639e-03	(4,8,0)	-8.666992e-04	(8,10,6)	-9.124881e-06		

TABLE V: Series coefficients for the magnon dispersion on the triangular lattice $J_z = 1$, $J_\perp = -1$, nonzero coefficients up to r=9 are listed for compactness (the complete series can be found in Ref. 23)

(r,m,n)	$c_{r,m,n}$	(r,m,n)	$c_{r,m,n}$	(r,m,n)	$c_{r,m,n}$	(r,m,n)	$c_{r,m,n}$
(0,0,0)	3.000000e+00	(8,4,2)	1.641818e-02	(8,7,3)	-3.898852e-03	(6,10,2)	-1.174079e-03
(2,0,0)	-1.250000e-01	(4,5,1)	-7.072545e-02	(6,7,5)	-4.696316e-04	(8,10,2)	-2.957178e-03
(4,0,0)	8.773202e-02	(6,5,1)	-2.266297e-02	(8,7,5)	-2.220857e-03	(8,10,4)	-1.051498e-03
(6,0,0)	-3.747008e-02	(8,5,1)	1.641818e-02	(4,8,0)	-3.632812e-03	(8,10,6)	-5.518909e-05
(8,0,0)	2.658737e-02	(4,5,3)	-1.453125e-02	(6,8,0)	-1.296471e-02	(6,11,1)	-4.696316e-04
(2,2,0)	-1.000000e-00	(6,5,3)	-1.709052e-02	(8,8,0)	-2.634458e-03	(8,11,1)	-2.220857e-03
(4,2,0)	3.067262e-01	(8,5,3)	-1.306500e-05	(6,8,2)	-8.548979e-03	(8,11,3)	-1.051498e-03
(6,2,0)	-1.478629e-01	(4,6,0)	-4.674479e-02	(8,8,2)	-3.898852e-03	(8,11,5)	-1.103782e-04
(8,2,0)	1.192248e-01	(6,6,0)	-2.107435e-02	(6,8,4)	-1.174079e-03	(6,12,0)	-7.827194e-05
(2,3,1)	-7.500000e-01	(8,6,0)	8.083746e-03	(8,8,4)	-2.957178e-03	(8,12,0)	-1.178397e-03
(4,3,1)	8.683532e-02	(4,6,2)	-2.179687e-02	(8,8,6)	-3.787294e-04	(8,12,2)	-7.614846e-04
(6,3,1)	-7.198726e-02	(6,6,2)	-1.775987e-02	(6,9,1)	-5.919357e-03	(8,12,4)	-1.379727e-04
(8,3,1)	6.383529e-02	(8,6,2)	1.136255e-03	(8,9,1)	-4.075885e-03	(8,13,1)	-3.787294e-04
(2,4,0)	-3.750000e-01	(6,6,4)	-5.919357e-03	(6,9,3)	-1.565439e-03	(8,13,3)	-1.103782e-04
(4,4,0)	-2.357440e-02	(8,6,4)	-4.075885e-03	(8,9,3)	-3.182356e-03	(8,14,0)	-1.146580e-04
(6,4,0)	-4.667627e-02	(4,7,1)	-1.453125e-02	(8,9,5)	-7.614846e-04	(8,14,2)	-5.518909e-05
(8,4,0)	4.476721e-02	(6,7,1)	-1.709052e-02	(8,9,7)	-1.576831e-05	(8,15,1)	-1.576831e-05
(4,4,2)	-7.072545e-02	(8,7,1)	-1.306500e-05	(6,10,0)	-2.499303e-03	(8,16,0)	-1.971039e-06
(6,4,2)	-2.266297e-02	(6,7,3)	-8.548979e-03	(8,10,0)	-3.646508e-03		

TABLE VI: Series coefficients for the magnon dispersion on the triangular lattice $J_z = 2$, $J_\perp = -1$, nonzero coefficients up to r=9 are listed for compactness (the complete series can be found in Ref. 23)

(r,m,n)	$c_{r,m,n}$	(r,m,n)	$c_{r,m,n}$	(r,m,n)	$c_{r,m,n}$	(r,m,n)	$c_{r,m,n}$
(0,0,0)	3.000000e+00	(6,5,1)	-5.113269e-01	(5,8,0)	1.114660e-01	(9,10,6)	3.094665e-02
(2,0,0)	-2.812500e-01	(7,5,1)	3.541550e-01	(6,8,0)	-2.789923e-01	(9,10,8)	4.332352e-04
(3,0,0)	-6.234375e-02	(8,5,1)	-5.927875e-01	(7,8,0)	3.889189e-01	(6,11,1)	-1.020493e-02
(4,0,0)	3.427127e-01	(9,5,1)	1.818953e+00	(8,8,0)	-5.937472e-01	(7,11,1)	5.778696e-02
(5,0,0)	1.248868e-01	(4,5,3)	-9.659180e-02	(9,8,0)	1.024914e+00	(8,11,1)	-1.791293e-01
(6,0,0)	-3.138557e-01	(5,5,3)	2.102338e-01	(5,8,2)	5.215530e-02	(9,11,1)	3.824414e-01
(7,0,0)	-2.065582e-01	(6,5,3)	-3.793451e-01	(6,8,2)	-1.818856e-01	(7,11,3)	1.646341e-02
(8,0,0)	2.679692e-01	(7,5,3)	4.434905e-01	(7,8,2)	3.088576e-01	(8,11,3)	-8.048695e-02
(9,0,0)	6.130976e-01	(8,5,3)	-6.470161e-01	(8,8,2)	-5.178979e-01	(9,11,3)	2.165711e-01
(1,2,0)	1.500000e+00	(9,5,3)	1.205017e+00	(9,8,2)	8.731811e-01	(8,11,5)	-8.618625e-03
(2,2,0)	-2.250000e+00	(3,6,0)	6.539063e-02	(6,8,4)	-2.551233e-02	(9,11,5)	4.893766e-02
(3,2,0)	-2.013281e-01	(4,6,0)	-3.105654e-01	(7,8,4)	9.867811e-02	(9,11,7)	1.732941e-03
(4,2,0)	1.349036e+00	(5,6,0)	3.819521e-01	(8,8,4)	-2.507655e-01	(6,12,0)	-1.700822e-03
(5,2,0)	3.245835e-01	(6,6,0)	-4.794666e-01	(9,8,4)	4.867085e-01	(7,12,0)	2.057252e-02
(6,2,0)	-9.772865e-01	(7,6,0)	4.227344e-01	(7,8,6)	3.292682e-03	(8,12,0)	-9.194406e-02
(7,2,0)	-1.324972e+00	(8,6,0)	-6.511353e-01	(8,8,6)	-2.934241e-02	(9,12,0)	2.400559e-01
(8,2,0)	1.736288e+00	(9,6,0)	1.561357e+00	(9,8,6)	1.091019e-01	(7,12,2)	9.878045e-03
(9,2,0)	1.998149e+00	(4,6,2)	-1.448877e-01	(5,9,1)	2.607765e-02	(8,12,2)	-5.858223e-02
(2,3,1)	-1.687500e+00	(5,6,2)	2.496909e-01	(6,9,1)	-1.264872e-01	(9,12,2)	1.748291e-01
(3,3,1)	5.109375e-01	(6,6,2)	-4.028414e-01	(7,9,1)	2.546730e-01	(8,12,4)	-1.077328e-02
(4,3,1)	1.438694e-01	(7,6,2)	4.542205e-01	(8,9,1)	-4.585226e-01	(9,12,4)	5.664036e-02
(5,3,1)	4.631412e-01	(8,6,2)	-6.635572e-01	(9,9,1)	7.791699e-01	(9,12,6)	4.043528e-03
(6,3,1)	-7.686440e-01	(9,6,2)	1.278006e+00	(6,9,3)	-3.401644e-02	(7,13,1)	3.292682e-03
(7,3,1)	-2.673657e-01	(5,6,4)	2.607765e-02	(7,9,3)	1.163420e-01	(8,13,1)	-2.934241e-02
(8,3,1)	2.424913e-01	(6,6,4)	-1.264872e-01	(8,9,3)	-2.770943e-01	(9,13,1)	1.091019e-01
(9,3,1)	2.292894e+00	(7,6,4)	2.546730e-01	(9,9,3)	5.242482e-01	(8,13,3)	-8.618625e-03
(2,4,0)	-8.437500e-01	(8,6,4)	-4.585226e-01	(7,9,5)	9.878045e-03	(9,13,3)	4.893766e-02
(3,4,0)	4.425000e-01	(9,6,4)	7.791699e-01	(8,9,5)	-5.858223e-02	(9,13,5)	6.065292e-03
(4,4,0)	-3.406189e-01	(4,7,1)	-9.659180e-02	(9,9,5)	1.748291e-01	(7,14,0)	4.703831e-04
(5,4,0)	5.419257e-01	(5,7,1)	2.102338e-01	(8,9,7)	-1.231232e-03	(8,14,0)	-8.933341e-03
(6,4,0)	-6.661367e-01	(6,7,1)	-3.793451e-01	(9,9,7)	1.347384e-02	(9,14,0)	4.854225e-02
(7,4,0)	3.675761e-02	(7,7,1)	4.434905e-01	(5,10,0)	5.215530e-03	(8,14,2)	-4.309313e-03
(8,4,0)	-2.016564e-01	(8,7,1)	-6.470161e-01	(6,10,0)	-5.380211e-02	(9,14,2)	3.094665e-02
(9,4,0)	2.293150e+00	(9,7,1)	1.205017e+00	(7,10,0)	1.541458e-01	(9,14,4)	6.065292e-03
(3,4,2)	1.961719e-01	(5,7,3)	5.215530e-02	(8,10,0)	-3.358010e-01	(8,15,1)	-1.231232e-03
(4,4,2)	-4.619167e-01	(6,7,3)	-1.818856e-01	(9,10,0)	6.055844e-01	(9,15,1)	1.347384e-02
(5,4,2)	4.570889e-01	(7,7,3)	3.088576e-01	(6,10,2)	-2.551233e-02	(9,15,3)	4.043528e-03
(6,4,2)	-5.113269e-01	(8,7,3)	-5.178979e-01	(7,10,2)	9.867811e-02	(8,16,0)	-1.539040e-04
(7,4,2)	3.541550e-01	(9,7,3)	8.731811e-01	(8,10,2)	-2.507655e-01	(9,16,0)	3.577909e-03
(8,4,2)	-5.927875e-01	(6,7,5)	-1.020493e-02	(9,10,2)	4.867085e-01	(9,16,2)	1.732941e-03
(9,4,2)	1.818953e+00	(7,7,5)	5.778696e-02	(7,10,4)	1.646341e-02	(9,17,1)	4.332352e-04
(3,5,1)	1.961719e-01	(8,7,5)	-1.791293e-01	(8,10,4)	-8.048695e-02	(9,18,0)	4.813724e-05
(4,5,1)	-4.619167e-01	(9,7,5)	3.824414e-01	(9,10,4)	2.165711e-01		
(5,5,1)	4.570889e-01	(4,8,0)	-2.414795e-02	(8,10,6)	-4.309313e-03		